Nanoscale

PAPER

View Article Online
View Journal | View Issue

Cite this: *Nanoscale*, 2025, **17**, 14164

Design of colloidal vectors for active targeting *via* complexation of biotinylated copolymers with gadolinium ions†

Maksym Odnoroh, [a] Franck Desmoulin, [b,c] Olivier Coutelier, [a] Carine Pestourie, [c] Christophe Mingotaud, [a] Mathias Destarac *[a] and Jean-Daniel Marty *[a]

Received 6th March 2025,
Accepted 15th May 2025

DOI: 10.1039/d5nr00986c

rsc.li/nanoscale

This study presents the design of biotin-functionalized hybrid polyionic complexes (HPICs) using RAFT polymers for MRI applications. The synthesized colloidal vectors, complexed with gadolinium ions, demonstrate high stability, relaxivity, and biotin accessibility for active targeting. Preliminary *in vivo* studies confirm their potential for improved MRI contrast and pharmacokinetic tracking.

Introduction

Over the past century, medical progress has been driven by the development of new drugs to improve therapeutics. However, in areas like cancer, outcomes often do not match the level of research due to issues with pharmacokinetics and pharmacodynamics, leading to drug elimination or severe side effects. To address these challenges, nanovectors—colloidal systems made of small molecules, polymers, or nanoparticles—have been developed. These systems, ranging from 10 nm to 1 μm, encapsulate drugs to protect them, control their release, reduce toxicity, and improve targeting. Nanovectors have evolved across three generations. The first generation involves simple colloids, like liposomes or nanoparticles, enabling passive drug delivery, with some modified to avoid immune clearance. The second generation employs active targeting *via* ligand–receptor interactions, while the third generation focuses on overcoming biological barriers and coordinating complex functions. Despite some progress, achieving precise targeting of diseased cells remains a significant challenge.[1] To achieve this, different vectorization strategies can be employed. The first one involves functionalizing preformed vectors, requiring specific surface functionalities and experimental conditions suitable for such chemical modifications. The second strategy relies on the prior modification of the molecules that constitute, upon assembly, these vectors.

In this context, the modification of polymeric structures is of particular interest, since various functional groups being bio-relevant can be incorporated into their architecture.[2] These groups may be distributed randomly along the polymer chain, positioned at the chain ends, or confined to a specific block within a block copolymer. Precise control over the placement of functional groups could be essential for optimizing biological properties of the polymer or its assembly. As a result, there is a growing demand for advanced synthetic methodologies to design polymers with enhanced precision. Reversible-deactivation radical polymerization (RDRP) is one such powerful tool.[3,4] Among different techniques, reversible addition–fragmentation chain transfer (RAFT)[5] polymerization has a particular interest, as it stands out for its broad compatibility with nearly all free-radical monomers and its straightforward implementation.

Polymers synthesized *via* RAFT polymerization can incorporate a wide variety of functional groups, making them particularly relevant for biomedical applications.[6–8] The nature and position of the functional group along the polymer chain dictate the synthetic strategy employed, whether by direct polymerization of functional monomers,[9–11] post-polymerization modification,[12,13] or use of RAFT agents bearing the desired functionality.[5,11,14,15] RAFT agents (of general structure R–S–(C═S)–Z) with functional R or Z groups enable precise placement of functional groups at the α- or ω-chain ends of polymers, facilitated by commercially available functional RAFT agents that are easily modified *via* simple reactions (*e.g.*, esterification[16] or amidation[17]). Additionally, RAFT terminal groups can be chemically transformed *via* post-polymerization, such as converting xanthates or trithiocarbonate RAFT end-groups into thiol groups *via* aminolysis, which can then undergo Michael addition reactions.[18,19]

One notable functional group is biotin (vitamin B_7), which is widely used in biochemistry due to its exceptionally strong

[a]*Université de Toulouse, CNRS UMR 5623, Laboratoire Softmat, Toulouse, France. E-mail: mathias.destarac@univ-tlse3.fr, jean-daniel.marty@univ-tlse3.fr*
[b]*Toulouse NeuroImaging Center (ToNIC), UMR 1214, Inserm, University of Toulouse – Paul Sabatier, Toulouse, France*
[c]*CREFRE-Anexplo, University of Toulouse, Inserm, UT3, ENVT, Toulouse, France*
† Electronic supplementary information (ESI) available. See DOI: https://doi.org/10.1039/d5nr00986c

ligand–protein interactions with avidin and streptavidin.[20,21] These interactions, with dissociation constants (K_d) of ~10^{-15} and 10^{-13} M, respectively, have broad applications including cancer diagnosis and treatment,[22,23] biosensors,[24] fluorescence-activated cell sorting (FACS),[25] cell-surface labeling,[26] bioconjugation,[27] and nanoparticle modification.[28] α-Biotinylated polymers can be synthesized using biotin-functionalized RAFT agents, typically obtained *via* 2-step esterification of both biotin and carboxylic acid-terminated chain transfer agents (CTAs) *via* bifunctional linkers.[29,30] Alternatively, biotinylation can occur by post-polymerization modification, for instance through amidation between *N*-(5-aminopentyl)biotinamide and a carboxy-terminated RAFT polymer[31] or *via* Michael addition of thiol-functionalized polymers (derived from the aminolysis of trithiocarbonate groups) with biotin-maleimide.[18] While some biotinylated polymers based on poly (ethylene glycol) (PEG-biotin) are commercially available but expensive and limited in PEG chain lengths, starting from biotinylated RAFT agents offers a more versatile and cost-effective approach, applicable to various monomers and targeted molar masses.

In this work, the objective is to design functional vectors by the complexation of biotin-modified double hydrophilic block copolymers (DHBCs) with metal ions, leading to the formation of hybrid polyionic complexes (HPICs) with biotin functionalities on their surface. Previously, non-functionalized HPICs have already showed their high potential as MRI contrast agents.[32–34] Biotin end-functional copolymers were obtained by RAFT polymerization, using biotinylated chain transfer agent (**B-CTA**). **B-CTA** was synthesized through a two-step process from biotin and a commercial RAFT agent, as illustrated in Scheme 1A and Scheme 2.

Consequently, the chosen block copolymer features a poly (oligo(ethylene glycol) methyl ether acrylate) (POEGA) block to ensure the stealth of the vector in biological media, and a complexing poly(vinylphosphonic acid) (PVPA) block. The phosphonic function exhibits enhanced affinity for ions of interest compared to that achieved using poly(acrylic acid)-type blocks[32] and imparts significantly improved colloidal stability to the resulting vectors.[9,35,36] The resulting polymers will be analyzed for their role in forming Gd/HPICs for use as MRI contrast agents. By mixing double hydrophilic block copolymers with and without biotin-functionalized probes (B-POEGA-*b*-PVPA and POEGA-*b*-PVPA respectively), HPICs with a specific surface density of biotin can be prepared for targeted reactions with biological entities (Scheme 1B).

Results and discussion

B-CTA synthesis

The RAFT agent was obtained from the modification of 2-(butylthiocarbonothioylthio)propanoic acid (**CTA1**) with biotin. However, since both molecules possess carboxylic groups, an intermediate linker was necessary. Given the low average molar mass (M_n) requirements for HPICs applications, a small

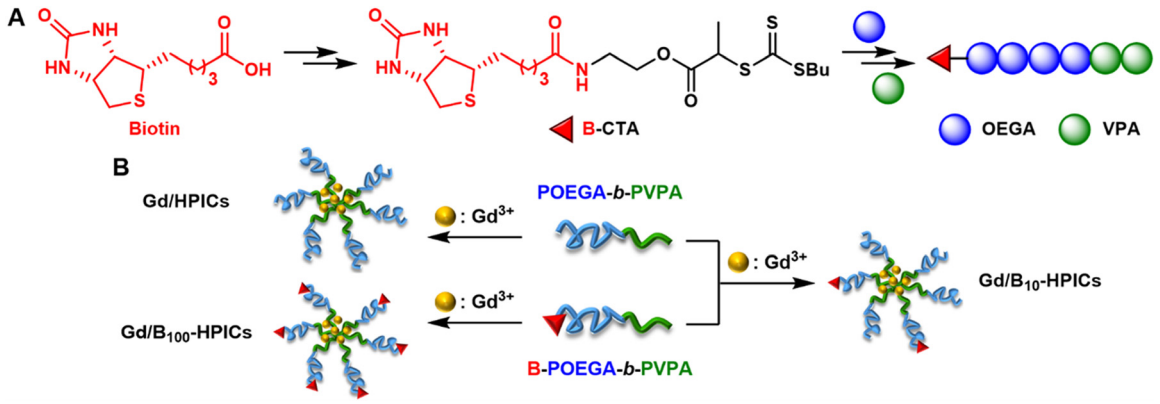

Scheme 1 (A) Synthesis of biotinylated RAFT agent (**B-CTA**) and corresponding diblock copolymer and (B) schematic representation of the formation of different HPICs types induced by the addition of Gd^{3+} ions to POEGA-*b*-PVPA (**Gd/HPICs**), B-POEGA-*b*-PVPA (**Gd/B_{100}-HPICs**) and their 90/10 mixture (**Gd/B_{10}-HPICs**) (B).

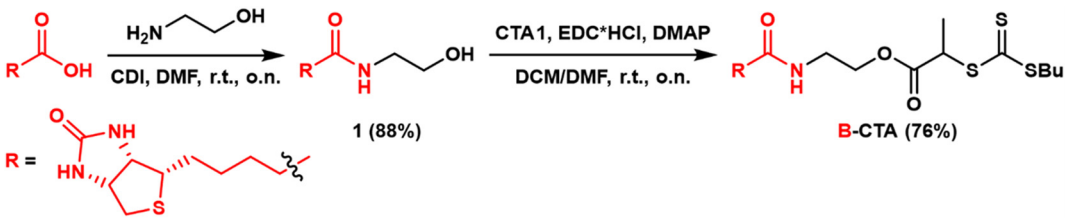

Scheme 2 Synthesis of **B-CTA**.

linker was deemed appropriate. This linker needed to have two nucleophilic groups with different reactivities to facilitate a two-step biotin modification without requiring additional protection/deprotection steps. Inspired by similar methodologies, such as the synthesis of biotinylated RAFT agents using 2-(2-aminoethoxy)ethanol as a linker and *S*-1-dodecyl-*S*′-(α,α′-dimethyl-α″-acetic acid) trithiocarbonate,[29] 2-aminoethanol and **CTA1** were used as the linker and commercial RAFT agent respectively. In the first step, biotin was converted into an amide intermediate with a high yield (88%, compound **1**) through a reaction with ethanolamine and 1,1′-carbonyldiimidazole (CDI) in DMF (Scheme 2, Fig. S1 and S2†). In the second step, compound **1** was modified with **CTA1** by esterification, using 1-ethyl-3-(3′-dimethylaminopropyl) carbodiimide (EDC·HCl) and 4-(dimethylamino)pyridine (DMAP). The reaction yielded a pure biotinylated RAFT agent (**B-CTA**) with a 76% yield (67% total yield across both steps) after column chromatography (Fig. S3 and S4†).

DHBCs synthesis

Oligo(ethylene glycol) methyl ether acrylate (OEGA) was selected as the neutral block due to the biocompatibility of POEGA[37] and because it can be polymerized by RAFT and afford a branched alternative to PEG, a gold standard in biological studies. PVPA was chosen as the ionizable block, based on its previously demonstrated capacity to form highly chemically stable HPICs. Two RAFT agents were used for this synthesis: **B-CTA** and methyl 2-(butylthiocarbonothioylthio)propanoate (**CTA2**) (Scheme 3).

The first block, POEGA, was synthesized *via* photo-iniferter RAFT polymerization using a handmade photoreactor equipped with blue LEDs (Fig. S11†). This methodology, previously employed by Mazo *et al.*, was selected to minimize side reactions during polymerization.[38] The reaction, targeting an M_n of approximately 3.6 kg mol^{-1}, was carried out in DMF (Scheme 3). After 48 hours, conversions of 91% (with **B-CTA**) and 88% (with **CTA2**) were achieved. The resulting polymers were purified by dialysis and lyophilization (Fig. S5 and S6†) prior to SEC analysis. Notably, POEGA polymers are known to interact with aqueous SEC columns,[11] leading to significant signal broadening and tailing (Fig. 1). For accurate M_n and dispersity ($Đ$) measurements, SEC was performed in THF, which revealed narrow, monomodal peaks (Fig. S12†). The obtained polymers, B-POEGA$_{3.6k}$ and POEGA$_{3.2k}$, exhibited $Đ$ values of 1.08 and 1.10, respectively. Aqueous SEC was subsequently employed to monitor chain extension during the synthesis of the second block, as PVPA cannot be analyzed by SEC in THF.

The chain extension with VPA was then carried out (Scheme 3). A target M_n of approximately 1.6–1.8 kg mol^{-1} was chosen for the second block to achieve an optimal ratio

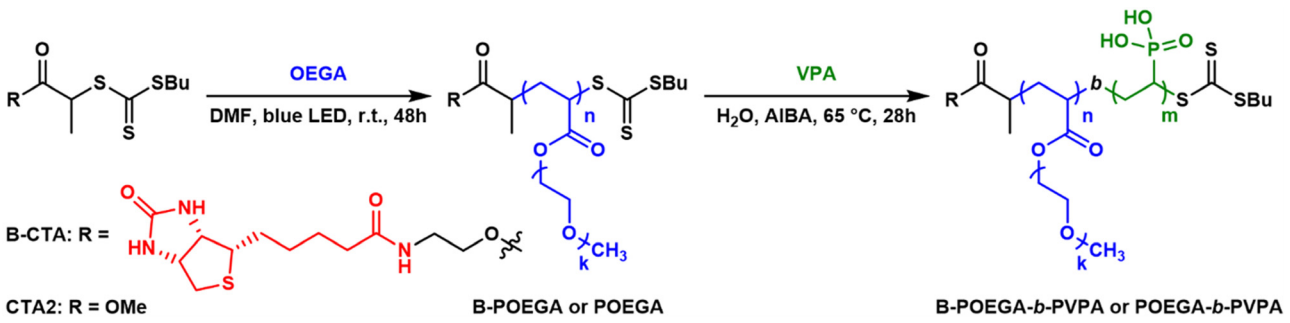

Scheme 3 Synthesis of DHBCs.

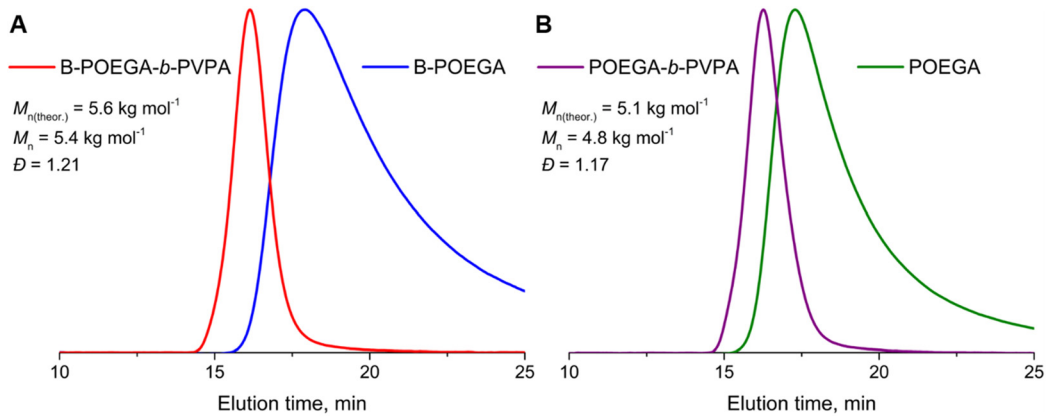

Fig. 1 Aqueous SEC-RI chromatograms of DHBCs and corresponding macro-CTA (A) B-POEGA-*b*-PVPA and B-POEGA; (B) POEGA-*b*-PVPA and POEGA.

between neutral and ionizable blocks for HPICs formation.[39] These values also represent the upper M_n limit for attaining controlled PVPA synthesis *via* RAFT polymerization.[40] Polymerization of VPA was conducted in water using AIBA as an initiator. Due to the low reactivity of VPA, the initiator concentration was set to 0.6 eq. relative to macro-CTA. After 28 hours, conversions of 42% (for B-POEGA$_{3.6k}$) and 38% (for POEGA$_{3.2k}$) were achieved. The polymers were purified *via* dialysis and lyophilization (Fig. S7–S10†), followed by aqueous SEC analysis (Fig. 2). The results showed monomodal peaks, with excellent agreement between the theoretical M_n and experimental values. Narrow dispersities were observed ($Đ$ = 1.21 and 1.17 for B-POEGA$_{3.6k}$-*b*-PVPA$_{1.8k}$ and POEGA$_{3.2k}$-*b*-PVPA$_{1.6k}$, respectively), confirming the successful synthesis of well-defined DHBCs.

HPICs formation and characterization

Three HPIC systems based on gadolinium were formulated, differing in the amount of biotin functionality present on their surface. They are obtained by mixing different proportions of DHBCs (B-POEGA-*b*-PVPA and POEGA-*b*-PVPA) with and without biotin-functionalized probes, as illustrated in Scheme 1. **Gd/HPICs** does not contain any biotin functionality, while the other two contain 10% and 100% (in number) of biotinylated copolymer, respectively, and are denoted as **Gd/B$_{10}$-HPICs** and **Gd/B$_{100}$-HPICs**.

The preparation of these gadolinium-based HPICs was initiated by the addition of a chosen volume of a concentrated solution of Gd^{3+} ions to a 0.5 wt% aqueous solution of chosen DHBCs. The mixture was characterized by the ratio (R), defined as the ratio of positive charges from the trivalent Gd^{3+} ions to the potentially available negative charges from the ionizable VPA units of the polymer: $R = 3[Gd^{3+}]/[VPA]$. The effect of the addition of increasing concentration of Gd^{3+} ions (equivalent to increasing R ratio) to a given concentration of polymer was monitored using mono-angle dynamic light scattering as illustrated in Fig. 2A in the case of **Gd/B$_{10}$-HPICs** (for **Gd/HPICs** and **Gd/B$_{100}$-HPICs** see Fig. S13†). Whatever the biotin content may be, a similar trend was recorded: at low R values, the formation of poorly defined aggregates with large Z-average diameters was observed, accompanied by a low scattered signal. For all studied systems, the scattering intensity increased for ratio up to 1 and then a plateau was reached for the measured value with a constant Z-averaged diameter. The Z-average values obtained, although consistent, do not accurately reflect the true size of the structures formed due to the presence of a minor population of large particles (100–1000 nm). To determine the actual hydrodynamic diameter of the particles in solution, the autocorrelation function from dynamic light scattering (DLS) measurements is analyzed to extract the number-weighted size distribution. At R = 1, hydrodynamic radii of the different systems were estimated from the calculated distribution (Fig. 2B) at 4.0 ± 0.3 nm, 4.1 ± 0.7 nm and 4.5 ± 0.4 nm for **Gd/HPICs**, **Gd/B$_{10}$-HPICs** and **Gd/B$_{100}$-HPICs** respectively (Table 1). Hence, the insertion of end-terminated biotin within HPICs structure does not modify significantly the overall size of the HPICs formed. Moreover, very low zeta potential values (between 1.6 and 1.9 mV, see Table 1) were measured. These observations are consistent with the formation of so-called core–shell HPICs structures, upon interaction between Gd^{3+} ions and the polymer chains. These colloids have been extensively described in the literature[32,41–43] and are here composed of PVPA blocks crosslinked by gadolinium ions, forming the core surrounded by a POEGA shell.

The chemical stability of the resulting colloids was investigated as a function of pH using DLS measurements (Fig. S14†). No significant changes in the measured hydrodynamic diameter were observed, indicating high stability of the HPICs over the studied pH range. This stability is attributed to the strong coordination between VPA units and lanthanide

Table 1 Main characteristics of Ln^{3+}/HPICs

Colloidal system	R_h, nm	ζ, mV	r_1, mM^{-1} s^{-1}	$n(H_2O)$
Ln/HPICs	4.0 ± 0.3	1.8 ± 0.5	34 ± 1	2.7 ± 0.1
Ln/B$_{10}$-HPICs	4.1 ± 0.7	1.9 ± 0.6	34 ± 1	2.7 ± 0.1
Ln/B$_{100}$-HPICs	4.5 ± 0.4	1.6 ± 0.6	35 ± 1	2.8 ± 0.1

R_h, ζ, and r_1 values were obtained for HPICs with Gd^{3+} ions; $n(H_2O)$ values were obtained for HPICs with Eu^{3+} ions.

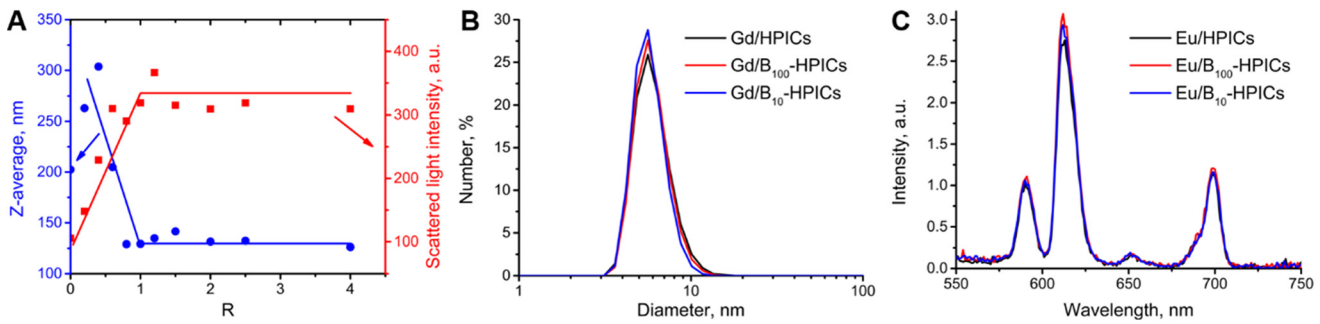

Fig. 2 (A) Evolution of Z-Average and scattered light intensity measured by DLS for an aqueous solution of **Gd/B$_{10}$-HPICs** as a function of ratios R ([polymer] = 0.5 wt%; lines are just guide for the eye). (B) Number-averaged hydrodynamic diameter distributions of **Gd/HPICs**, **Gd/B$_{100}$-HPICs** and **Gd/B$_{10}$-HPICs** (R = 1). (C) Emission spectra of **Eu/HPICs**, **Eu/B$_{100}$-HPICs** and **Eu/B$_{10}$-HPICs** at R = 1.

ions, which confers excellent robustness to the PVPA-based HPICs in both buffered environments and saline solutions.[35] The *in vitro* relaxation properties of the different systems were measured at 0.47 T and 25 °C (Table 1). Measured specific relaxivities values are high (34 ± 1 mM^{-1} s^{-1}) and comparable to those of PEO_{2k}-*b*-$PVPA_{1k}$ (32 ± 1 mM^{-1} s^{-1}), but remarkably higher compared to standard molecular complexes like DOTAREM® (r_1 = 3.4 mM^{-1} s^{-1}).[44] Additionally, the number of coordinated water molecules was determined for HPICs, replacing Gd^{3+} with Eu^{3+} ions and analyzing Eu^{3+} emission spectra (Fig. 2C) and fluorescence lifetimes. Using the equation proposed by Supkowski *et al.*,[45] the calculated number of coordinated water molecules was 2.7–2.8 (Table 1). This value is significantly lower than the nine water molecules expected for fully hydrated europium salt in water.[46]

In vitro biotin binding

The different HPICs systems vary in the level of biotin functionality located on the outer corona. Nonetheless, various physicochemical measurements indicate that these different systems share similar properties in terms of size, stability, relaxivity and microstructure. The objective now is to demonstrate the ability of HPICs structure to achieve active targeting due to the presence of biotin. Although the strong interaction between biotin and avidin is well-documented, it was necessary to confirm that when DHBCs form HPICs, biotin remains accessible and can interact with specific targets.

To evaluate the targeting capabilities of modified polymers, the ability of **Eu/B_{10}-HPICs** to bind to avidin, a tetrameric protein, was assessed and compared to that of pure biotin and the block copolymer bearing the biotin functionality (Fig. S15†). In this study, Eu^{3+} ions were used instead of Gd^{3+} to monitor Eu^{3+} intensity through fluorimetry. For this purpose, avidin was pre-bound to 4′-hydroxyazobenzene-2-carboxylic acid (HABA). When bound, the HABA-avidin complex exhibits strong absorption at 500 nm, whereas free HABA absorbs at 348 nm (Fig. S16†). Given that the biotin–avidin interaction is significantly stronger, biotin can displace HABA, resulting in a decrease in the 500 nm absorption band. By measuring this decrease, the amount of accessible biotin in the solution can be quantified.[47] In the presence of different concentrations of pure biotin, a linear increase of measured binding efficiency was measured (Fig. S17† and blue line in Fig. 3). The same experiment was repeated using B-$POEGA_{3.6k}$-*b*-$PVPA_{1.8k}$ block copolymer at the same biotin concentration to evaluate biotin availability at the chain ends (Fig. 3 and Fig. S18†). The binding efficiency for the copolymer was only 41% of that observed with pure biotin, likely due to steric hindrance of the expected random coil conformation of the polymer in solution, which may limit biotin accessibility. In the case of **Eu/B_{10}-HPICs** (Fig. 3 and Fig. S19†), the binding efficiency was higher than that measured for the copolymer alone, reaching 58%. This improvement is attributed to conformational constraints within the HPICs, which force biotin groups to orient towards the periphery, thereby enhancing accessibility.

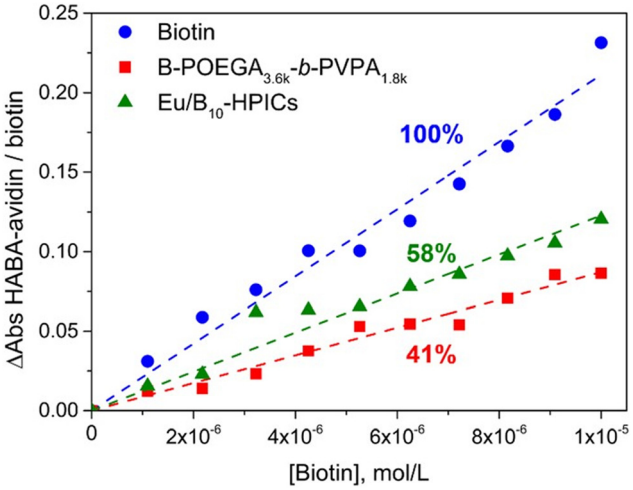

Fig. 3 Comparison of the binding efficiency of biotin to avidin at different concentrations for pure biotin (blue circles), biotin grafted on B-$POEGA_{3.6k}$-*b*-$PVPA_{1.8k}$ block copolymer (red squares) (DHBCs) or **Eu/B_{10}-HPICs** (green triangles) (HPICs).

To confirm that the integrity of the HPICs was maintained, fluorimetry measurements were performed (Fig. S20A†). The emission spectra are characteristic of complexed Eu^{3+} ions. The peaks at 590 nm and 615 nm correspond to the $^5D_0 \rightarrow {}^7F_1$ and $^5D_0 \rightarrow {}^7F_2$ transitions, respectively. The intensity ratio among the emission bands at 590, 610, and 700 nm remained consistent across different *R* values, reflecting the typical spectral profile of Eu/HPICs complexes. The overall luminescence intensity increased linearly with the concentration of added HPICs solution, while the emission band ratio between 590 and 610 nm remained unchanged throughout the experiment (Fig. S20B†). This constant ratio matches that of pure Eu/HPICs, confirming the structural integrity of the complexes during the measurements.

Small animal MRI

Previous experiments with HPICs conducted in cell culture medium using human colorectal tumour cells (HCT-116) demonstrated low cytotoxicity, even at high concentrations, for HPICs featuring a PEG-based outer shell.[33,41] Based on these findings, *in vivo* experiments were conducted in mice to obtain preliminary assessments of MRI contrast efficacy, pharmacokinetic properties, and tolerance. MRI contrast was evaluated following intravenous (IV) bolus injection of **Gd/B_{10}-HPICs** or **Gd/HPICs** at R = 0.8 ensuring the absence of free Gd(III) ions.[32,35] Tissue uptake and elimination properties were evaluated using a *T*1-weighted dynamic sequence of coronal images centered on the abdominal cavity, acquired over ~70 min after IV injection of HPICs at a dose equivalent to 15 μmol Gd per kg. Signal intensity changes were monitored in several regions of interest (ROIs), including the renal medulla, bladder, vascular space (blood), liver, and spleen (Fig. 4). Dynamics of signal intensities in mouse tissues were similar between **Gd/B_{10}-HPICs** and **Gd/HPICs** (Fig. 4 and Fig. S21†). Following HPICs

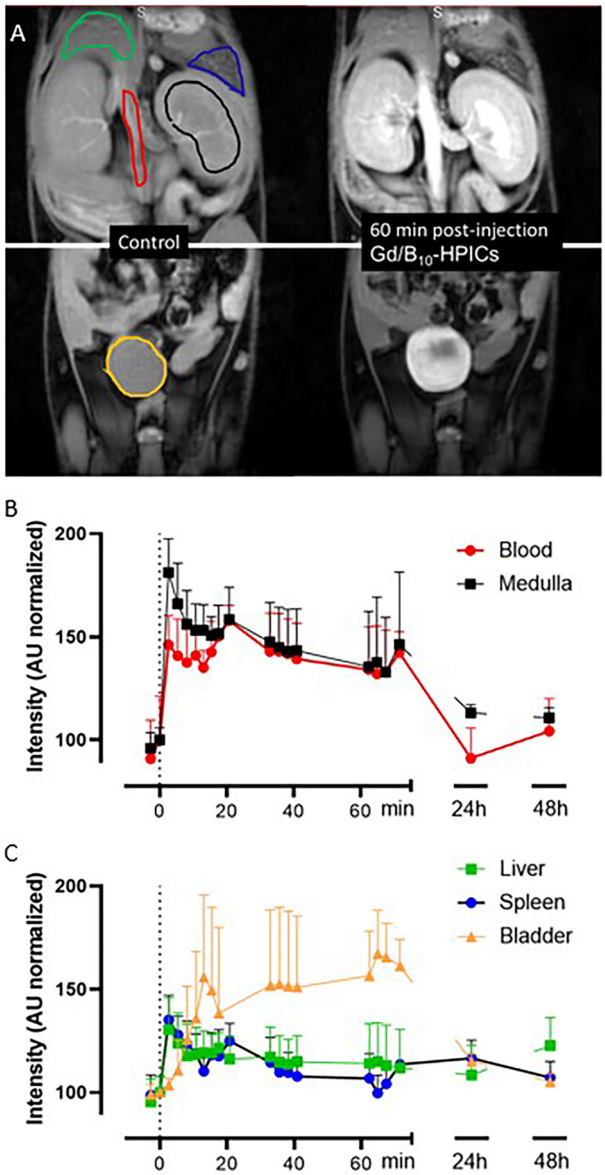

Fig. 4 Dynamics of signal intensities in mouse tissues following the administration of **Gd/B_{10}-HPICs**. Representative horizontal abdominal slices showing the kidneys, liver, spleen, lower aorta (top), and bladder (bottom), acquired before (left) and 60 minutes after intravenous injection of **Gd/B_{10}-HPICs** (right) (A). Regions of interest (ROIs) are outlined: renal medulla (black), vascular space (red), spleen (blue), liver (green), and bladder (orange). Time evolution of normalized signal intensities over 48 hours in the vascular space (blood) and renal medulla (B). Time evolution of normalized signal intensities over 48 hours in the liver, spleen, and bladder (C). Vertical dotted lines indicate the time of injection.

injection, a sharp increase in signal intensity was observed in all organs, except for the bladder content, indicating the systemic distribution of the contrast agents. Within the first five minutes, signal intensity increased by about 80% in the renal medulla and 50% in the blood, while liver and spleen signals peaked at about 40% above baseline, with no significant differences between the two HPICs. Urinary excretion exhibited a delayed onset, beginning approximately five minutes post-injection. Signal intensities in the renal medulla and blood remained at similar levels at 60 minutes, suggesting a half-life of several hours. This is notably longer than that of Gd-DOTA, a widely used clinical contrast agent, which has a reported half-life of 13 minutes in mice,[48] indicating a distinct pharmacokinetic profile, as intended. Images acquired 24- and 48-hours post-injection showed a return of signal intensities to baseline levels, suggesting that HPICs are likely eliminated through multiple pathways, which remain to be determined. As anticipated, due to their similar hydrodynamic radii and equivalent gadolinium content, both **Gd/HPICs** and **Gd/B_{10}-HPICs** exhibited comparable dynamics of signal intensity within mouse tissues. Had a targeting agent such as streptavidin been employed, a distinct and localised signal enhancement in specific tissues would have been expected with **Gd/B_{10}-HPICs**. The animals were kept under observation in the animal facility for 15 days post-injection, and no signs of acute toxicity were reported.

Conclusions

In this study, novel hybrid polyionic complexes (HPICs) were used as biotin-based colloidal vectors. These HPICs were obtained by mixing a biotin-terminated double hydrophilic block copolymer (DHBC) and a non-modified DHBC with lanthanide ions (Gd^{3+} or Eu^{3+}). DHBCs were obtained by RAFT polymerization using a biotin-functionalized chain transfer agent (**B-CTA**) with oligo(ethylene glycol) methyl ether acrylate (OEGA) as the neutral block and vinyl phosphonic acid (VPA) as the ionizable block. The obtained HPICs were characterized using dynamic light scattering (DLS) and fluorimetry, demonstrating high chemical stability across different pH values. The HPICs also exhibited high relaxivity values, underscoring their potential as MRI contrast agents.

Additionally, *in vitro* studies using avidin as a specific target confirmed the accessibility of biotin moieties in both the DHBCs and HPICs. This accessibility could enhance MRI resolution by enabling targeted imaging. Preliminary *in vivo* studies of the HPICs revealed an increased contrast and allowed tracking of their pharmacokinetics. Further *in vivo* studies are planned to evaluate the potential of these HPICs for specific-targeted MRI applications.

Author contributions

Conceptualization: J.-D. M., M.D., C.M., O.C.; experimentation: M. O., F.D., C.P.; supervision: J.-D. M., M.D., C.M., O.C.; writing: M.O., F.D., J.-D. M., M.D., C.M., O.C.

Data availability

The data supporting this article (materials and methods, complementary data) have been included as part of the ESI.†

Conflicts of interest

There are no conflicts to declare.

Acknowledgements

The authors thank Pascale Laborie (Technopolym, Institut de Chimie de Toulouse, UAR 2599) for her help with aqueous SEC analysis, Magali Albignac for preliminary experiments and CREFRE-Oncopole Experimental zootechny team (Inserm CREFRE-Anexplo, Toulouse France) for animal care and housing. This work was supported by the ANR agency under grant Hybrid-MRI (ANR-19-CE09-0011-01), which is gratefully acknowledged.

All *in vivo* experimental procedures were approved by our institutional animal care and use committee CEEA122 (APAFIS 34703-2022011811542488) and conducted in compliance with the Ethics Committee pursuant to European legislation translated into French Law as Décret 2013-118 dated 1st of February 2013.

References

1 M. Beija, R. Salvayre, N. L. Viguerie and J.-D. Marty, *Trends Biotechnol.*, 2012, **30**, 485–496.
2 K. Matyjaszewski and N. V. Tsarevsky, *Nat. Chem.*, 2009, **1**, 276–288.
3 N. Corrigan, K. Jung, G. Moad, C. J. Hawker, K. Matyjaszewski and C. Boyer, *Prog. Polym. Sci.*, 2020, **111**, 101311.
4 M. Destarac, *Polym. Chem.*, 2018, **9**, 4947–4967.
5 S. Perrier, *Macromolecules*, 2017, **50**, 7433–7447.
6 J. Nicolas, S. Mura, D. Brambilla, N. Mackiewicz and P. Couvreur, *Chem. Soc. Rev.*, 2013, **42**, 1147–1235.
7 C. Boyer, V. Bulmus, T. P. Davis, V. Ladmiral, J. Liu and S. Perrier, *Chem. Rev.*, 2009, **109**, 5402–5436.
8 B. D. Fairbanks, P. A. Gunatillake and L. Meagher, *Adv. Drug Delivery Rev.*, 2015, **91**, 141–152.
9 K. H. Markiewicz, L. Marmuse, M. Mounsamy, C. Billotey, M. Destarac, C. Mingotaud and J.-D. Marty, *ACS Macro Lett.*, 2022, 1319–1324.
10 M. Semsarilar and V. Abetz, *Macromol. Chem. Phys.*, 2021, **222**, 2000311.
11 M. Odnoroh, J.-D. Marty, V. Bourdon, O. Coutelier and M. Destarac, *Polym. Chem.*, 2023, **14**, 3821–3826.
12 X. Jiang, J. Zhang, Y. Zhou, J. Xu and S. Liu, *J. Polym. Sci., Part A: Polym. Chem.*, 2008, **46**, 860–871.
13 P. R. Bachler, M. D. Schulz, C. A. Sparks, K. B. Wagener and B. S. Sumerlin, *Macromol. Rapid Commun.*, 2015, **36**, 828–833.
14 K. T. Wiss, O. D. Krishna, P. J. Roth, K. L. Kiick and P. Theato, *Macromolecules*, 2009, **42**, 3860–3863.
15 H. T. Ho, F. Leroux, S. Pascual, V. Montembault and L. Fontaine, *Macromol. Rapid Commun.*, 2012, **33**, 1753–1758.
16 D. L. Patton and R. C. Advincula, *Macromolecules*, 2006, **39**, 8674–8683.
17 M. Bathfield, F. D'Agosto, R. Spitz, M.-T. Charreyre and T. Delair, *J. Am. Chem. Soc.*, 2006, **128**, 2546–2547.
18 Y.-Z. You and D. Oupický, *Biomacromolecules*, 2007, **8**, 98–105.
19 Z. An, W. Tang, M. Wu, Z. Jiao and G. D. Stucky, *Chem. Commun.*, 2008, 6501–6503.
20 M. Wilchek and E. A. Bayer, *Anal. Biochem.*, 1988, **171**, 1–32.
21 P. C. Weber, D. H. Ohlendorf, J. J. Wendoloski and F. R. Salemme, *Science*, 1989, **243**, 85–88.
22 H. Shi, C. Imberti, H. Huang, I. Hands-Portman and P. J. Sadler, *Chem. Commun.*, 2020, **56**, 2320–2323.
23 A. Jain and K. Cheng, *J. Controlled Release*, 2017, **245**, 27–40.
24 K. A. Edwards, H. A. Clancy and A. J. Baeumner, *Anal. Bioanal. Chem.*, 2006, **384**, 73–84.
25 A. Sardo, T. Wohlschlager, C. Lo, H. Zoller, T. R. Ward and M. Creus, *Protein Expression Purif.*, 2011, **77**, 131–139.
26 S. Fornera, T. E. Balmer, B. Zhang, A. D. Schlüter and P. Walde, *Macromol. Biosci.*, 2011, **11**, 1052–1067.
27 X. Wang, L. Liu, Y. Luo and H. Zhao, *Langmuir*, 2009, **25**, 744–750.
28 R. Narain, M. Gonzales, A. S. Hoffman, P. S. Stayton and K. M. Krishnan, *Langmuir*, 2007, **23**, 6299–6304.
29 C.-Y. Hong and C.-Y. Pan, *Macromolecules*, 2006, **39**, 3517–3524.
30 G. Gody, P. Boullanger, C. Ladavière, M.-T. Charreyre and T. Delair, *Macromol. Rapid Commun.*, 2008, **29**, 511–519.
31 A. Aqil, H. Qiu, J.-F. Greisch, R. Jérôme, E. De Pauw and C. Jérôme, *Polymer*, 2008, **49**, 1145–1153.
32 C. Frangville, Y. Li, C. Billotey, D. R. Talham, J. Taleb, P. Roux, J.-D. Marty and C. Mingotaud, *Nano Lett.*, 2016, **16**, 4069–4073.
33 M. Yon, L. Gibot, S. Gineste, P. Laborie, C. Bijani, C. Mingotaud, O. Coutelier, F. Desmoulin, C. Pestourie, M. Destarac, D. Ciuculescu-Pradines and J.-D. Marty, *Nanoscale*, 2023, **15**, 3893–3906.
34 M. Yon, L. Esmangard, M. Enel, F. Desmoulin, C. Pestourie, N. Leygue, C. Mingotaud, C. Galaup and J.-D. Marty, *Nanoscale*, 2024, **16**, 3729–3737.
35 M. Odnoroh, O. Coutelier, C. Mingotaud, M. Destarac and J.-D. Marty, *J. Colloid Interface Sci.*, 2023, **649**, 655–664.
36 M. Odnoroh, C. Mingotaud, O. Coutelier, J.-D. Marty and M. Destarac, *Eur. Polym. J.*, 2024, **210**, 112963.
37 J. A. A. Bogdanov, R. Weissleder, H. W. Frank, A. V. Bogdanova, N. Nossif, B. K. Schaffer, E. Tsai, M. I. Papisov and T. J. Brady, *Radiology*, 1993, **187**(3), 701–706.
38 A. R. Mazo, T. N. Tran, W. Zhang, Y. Meng, A. Reyhani, S. Pascual, L. Fontaine, G. G. Qiao and S. Piogé, *Polym. Chem.*, 2020, **11**, 5238–5248.
39 S. Gineste and C. Mingotaud, *Adv. Colloid Interface Sci.*, 2023, **311**, 102808.

40 I. Blidi, R. Geagea, O. Coutelier, S. Mazières, F. Violleau and M. Destarac, *Polym. Chem.*, 2012, **3**, 609–612.
41 M. Yon, S. Gineste, G. Parigi, B. Lonetti, L. Gibot, D. R. Talham, J.-D. Marty and C. Mingotaud, *ACS Appl. Nano Mater.*, 2021, **4**, 4974–4982.
42 L. Peng, M. Odnoroh, M. Destarac, Y. Coppel, C. Delmas, F. Benoit-Marquié, C. Mingotaud and J.-D. Marty, *Nanoscale*, 2025, **17**, 4636–4648.
43 K. H. Markiewicz, L. Seiler, I. Misztalewska, K. Winkler, S. Harrisson, A. Z. Wilczewska, M. Destarac and J.-D. Marty, *Polym. Chem.*, 2016, **7**, 6391–6399.
44 M. Rohrer, H. Bauer, J. Mintorovitch, M. Requardt and H.-J. Weinmann, *Invest. Radiol.*, 2005, **40**, 715–724.
45 R. M. Supkowski and W. DeW. Horrocks, *Inorg. Chim. Acta*, 2002, **340**, 44–48.
46 S. A. Cotton and P. R. Raithby, *Coord. Chem. Rev.*, 2017, **340**, 220–231.
47 D. Li, M. W. Frey, D. Vynias and A. J. Baeumner, *Polymer*, 2007, **48**, 6340–6347.
48 F. Bourasset, A. Dencausse, P. Bourrinet, M. Ducret and C. Corot, *MAGMA*, 2001, **12**, 82–87.